



Simulation of the 1953 storm surge in the North Sea

Byung Ho Choi¹ · Kyeong Ok Kim² · Jin-Hee Yuk³ · Han Soo Lee⁴

Received: 23 February 2018 / Accepted: 29 August 2018 / Published online: 15 September 2018
© Springer-Verlag GmbH Germany, part of Springer Nature 2018

Abstract

The 1953 North Sea floods, the Big Flood, was one of the worst natural disasters in Europe in modern times and is probably one of the most studied severe coastal floods. Several factors led to the devastating storm surge along the southern North Sea coast in combination of strong and sustained northerly winds, invert barometric effect, high spring tide, and an accumulation of the large surge in the Strait of Dover. However, the storm waves and their roles during the 1953 North Sea storm surge are not well investigated. Therefore, the effect of wave setup due to breaking waves in the storm surge processes is investigated through numerical experiments. A coupled process-based tide-wave-surge model was used to investigate and simulate the storm surge in the North Sea during January 31–February 1, 1953 and validated by comparing with historical water level records at tide gauges and wave observations at light vessels in the North Sea. Meteorological forcing inputs for the period, January 27–February 3, 1953 are reproduced from ERA-20C reanalysis data with a constant correction factor for winds. From the simulation results, it is found that, in addition to the high water due to wind setup, wave setup due to breaking waves nearshore play a role of approximately 10% of the storm surge peaks with approximately 0.2 m. The resulting modeling system can be used extensively for the preparedness of the storm surge and wave of extreme condition, and usual barotropic forecast.

Keywords Storm surge · The North Sea · Wave setup · Coupled wave-tide-surge model · Unstructured mesh · 1953 North Sea storm

1 Introduction

The 1953 North Sea floods, the Big Flood, was one of the worst natural disasters in Europe in modern times. The floods were caused by a deep low-pressure system (minimum

pressure 966 hPa) which moved rapidly southeast across the North Sea, causing strong northwesterly gales. Although not an especially deep system, it moved close to the land, giving sustained winds (over 50 knots for 24 h). The night of January 31 was a high spring tide, exacerbating the effects of the storm

This article is part of the Topical Collection on the *15th International Workshop on Wave Hindcasting and Forecasting in Liverpool, UK, September 10–15, 2017*

Responsible Editor: Jenny M Brown

Electronic supplementary material The online version of this article (<https://doi.org/10.1007/s10236-018-1223-z>) contains supplementary material, which is available to authorized users.

✉ Han Soo Lee
leehs@hiroshima-u.ac.jp

Byung Ho Choi
bhchoi.skku@gmail.com

Kyeong Ok Kim
kokim@kiost.ac.kr

Jin-Hee Yuk
jhyuk@kisti.re.kr

- ¹ Department of Civil and Environmental Engineering, Sungkyunkwan University, Suwon 16419, Republic of Korea
- ² Marine Environmental Research Center, Korea Institute of Ocean Science and Technology, Busan 49111, Republic of Korea
- ³ Division of National Supercomputing, Korea Institute of Science and Technology Information (KISTI), Daejeon 34141, Republic of Korea
- ⁴ Graduate School for International Development and Cooperation (IDEC), Hiroshima University, 1-5-1 Kagamiyama, Higashi-Hiroshima, Hiroshima 739-8529, Japan

surge. The floods hit on the night of January 31/February 1, 1953. In the UK, flooding was experienced over a 1000-mi stretch of coast all the way down the east coast, however the worst effects were in Essex and the Thames estuary (Wadey et al. 2015; Wolf and Flather 2005).

In some places, sea levels with 3 m above normal were recorded; 307 people died in southeast England, 58 in Canvey Island alone. An estimated 160,000 ha of land was flooded and over 24,000 homes destroyed. The estimated damage was around £50 million (at the time) (Muir Wood et al. 2005).

The damage was even worse in the Netherlands, with large parts of Zuid-Holland, Zeeland, and Nord Brabant being flooded, 200,000 ha in total. An estimated 1836 people lost their lives, mostly in Zeeland, and 100,000 more were evacuated. In Dutch, this event is known as the watersnoodramp (flood disaster) (Rijkswaterstaat and KNMI 1961). The floods also caused deaths and significant damage in Belgium (22 casualties) and Germany. Lives were also lost at sea during the storm (Gerritsen 2005).

In the UK, this event was a pivotal influence for flood risk management. Subsequent progress included a national tide gauge network, storm surge forecasting and warning service, and major defense upgrades such as the Thames Barrier which officially open in May 1984 (Wadey et al. 2015). In the Netherlands, just after the storm surge floods, the Delta Committee established on February 18, 1953 and submitted its main advice not only to close and heighten all existing dykes but also to realize the Dutch Deltawerken (delta works), so-called the Delta Plan. The key part of the plan was the full closure of the three northern inlets by an almost direct connection of the natural dunes to create a closed coastline. After 3 years and 5 months of the 1953 storm surge floods, the work on the Delta Plan was officially started and, in October 1986, was completed more than 33 years after the flood with major improvements in the eastern Scheldt from full damming to movable tidal barriers owing to pressure from fishing, oyster and mussel culture, and much increased environmental awareness (Gerritsen 2005). Further detailed descriptions on historical backgrounds, acute human impacts of the floods, aftermath and responses, and the lessons learned from the Netherlands and the UK sides are referred to Gerritsen (2005) and Baxter (2005), respectively, among many.

Since the Big Flood, scientific studies on meteorological conditions and the storm surge mechanism have also been reported based on observed data analysis and numerical modeling aspect (Flather 1984; Hansen 1956; Rossiter 1954; Schneider et al. 2013; Wadey et al. 2015; Wolf and Flather 2005). More lists of Dutch reports can also be found in Gerritsen (2005).

Earlier efforts to investigate the storm surge process were made by Rossiter (1954) based on the observed data analysis for winds and tides. He also conducted a prediction of the surge using surge prediction formula and made suggestions

for the improvement of surge prediction. Hansen (1956) proposed a methodology to calculate water level and currents and applied it to the entire North Sea for the 1953 storm surge event. By comparing with the Rossiter's water levels, Hansen (1956) illustrated possibility of water level and current prediction.

Flather (1984) later performed careful simulations of the 1953 storm surge in the North Sea using a finite difference model on a 36-km grid with required meteorological forcing reconstructed from a combination of surface pressure observations from the UK Meteorological Office (Met Office) daily weather report and values read from charts. Winds were estimated from the pressure distributions using empirical relations in Flather (1984), and the model reproduced the surges observed at the coast with good accuracy. Wolf and Flather (2005) made improved storm surge simulations on a 12-km grid with meteorological forcing with the same data and methods of Flather (1984), covering the North Sea and continental shelf. In Wolf and Flather (2005), they also made a simulation for waves in the North Sea using WAM model (WAMDI 1988) with the wind forcing from National Centers for Environmental Prediction/National Center for Atmospheric Research (NCEP/NCAR) reanalysis winds for the 1953 North Sea storm (<https://www.esrl.noaa.gov/psd/data/gridded/data.ncep.reanalysis.html>). The reconstructed and NCEP/NCAR winds were compared with observations from light vessels. The calculated maximum of the wave height at 00:00 GMT on February 1, 1953 was about 10 m in the southern North Sea. Due to the lack of wave records during the 1953 North Sea storm, it was difficult to compare their calculated results, but it was shown that the high wave fields could be an important factor during the 1953 storm surge floods. The surge-wave interaction was not taken into account in Wolf and Flather (2005).

In this study, we made waves and storm surge simulations of the 1953 North Sea storm surge event by using a high-resolution tide-surge-wave-coupled model with unstructured meshes. The tide-surge and wave models are synchronously coupled and the effects of waves on surge heights via wave setup due to wave breaking are considered in the shallow water. To the extent of authors' knowledge, the storm waves and their roles during the 1953 North Sea storm surge are not well investigated. Therefore, the objectives of this study are to reproduce the storm surge and waves during the 1953 North Sea storm and to investigate the effect of wave setup in the storm surge processes with the high-resolution tide-surge-wave-coupled model. The meteorological conditions, storm surge, and waves during the storm are described in Section 2, and the data and methodology are presented in Section 3. The results and discussion are described in Sections 4, followed by conclusion in Section 5. All times and all units of heights in this paper are in UTC and m, respectively.

2 Meteorological conditions, storm surge, and waves

The 1953 storm developed to the southeast of Greenland on January 28 and moved eastwards, crossing Scotland to the north, before traveling in a south-eastward path across the North Sea and into Germany (Wadey et al. 2015). The track of the depression from the Atlantic over the north Scotland into the North Sea, and the accompanying movement of the high-pressure system behind it, meant that powerful northerly winds swept down the eastern UK coast and the western part of the North Sea. The central pressure of the storm over the northern North Sea dropped to 964 hPa at 06:00–12:00 on January 31 (MetOffice 2014) that was at 1004 hPa at 12:00 on January 29. At 18:00 on January 31 when the storm's effects at the coast were becoming apparent, very strong northerly winds were generated over the North Sea, attribute to interaction with the high pressure (anticyclone) to the west of the UK (Fig. 1). On January 31, 1953, the wind speeds over 31 m/s were observed in Aberdeenshire (Wolf and Flather 2005), while the highest recorded 10 min mean wind speed at Stonehaven, Scotland, was 33.5 m/s from a northwest direction (Hickey 2001).

In comparison with other major historical storms and floods in the North Sea, the depression of the 1953 storm field was not exceptionally deep, but its storm track was different and its propagation somewhat slower. As a result, storm winds from the northeast were stronger and more sustained over a long north-south fetch, leading to a higher and more sustained surge and high-developed waves (Gerritsen 2005). By reaching the relatively shallow North Sea, this water is forced southwards, eventually causing a pile up of water in the south. This is because the water cannot escape through the narrow Dover Strait and the English Channel and so gets trapped in the southern North Sea. Then, the combination of high spring tides, storm surge, winds, and large waves resulted in sea defenses being overwhelmed in some locations, leading to extensive flooding.

Figure 2 shows the locations of tide gauges in the southern North Sea and the estimated track of the 1953 North Sea storm. Water levels during the storm surge event were recorded at the tide gauges of Fig. 2, whereas several tide gauges in the UK east coast failed during the storm. Rossiter (1954) collected all available tide gauge data and reported them as hourly time series, providing a valuable record of the observed sea levels during the storm surge. The tide gauge records from Rossiter (1954) are used for validation of storm surge model results in this study.

On the other hand, wave height measurements and records are sparse and often subjective and contradictory during the event in comparison with the tide gauge data (Wolf and Flather 2005). During the event, three light vessels (Dowsing: 53° 35' N, 0° 55' E; Smith's Knoll:

52° 43' N, 2° 18' E; Galloper: 51° 44' N, 1° 58' E) off the east coast of the UK recorded winds and waves. Maximum significant wave heights reported at the three locations were 3, 2.5, and 4.5 m, respectively. However, an ambiguity in the reporting scale means that, potentially, these waves could have been much higher. Wolf and Flather (2005) reported the visually observed wave heights at three light vessels and the possible “corrected” wave heights, assuming the alternative reading for the wave height code. The records of wave heights observations and their corrected values are used for model validation in Section 4.

3 Data and methodology

3.1 Meteorological forcing

For meteorological forcing, such as 10 m winds and surface pressure fields, of storm surge and wave modeling, three dataset, ERA-20C reanalysis (Poli et al. 2013), NCEP/NCAR Global Reanalysis Project (NNRP) (<https://rda.ucar.edu/datasets/ds090.0/>) WRF-downscaled data, and ERA-20C WRF-downscaled data, are compared and evaluated in terms of spatio-temporal variations of 10 m winds and pressure fields and resulting storm surges. To improve the 10 m winds and surface pressure fields further, three variations of ERA-20C reanalysis dataset with constant correction factors of 1.2, 1.35, and 1.5 for winds are also considered in the evaluation process. Based on the evaluation results of meteorological forcing, the ERA-20C reanalysis 10 m winds and pressure fields with a wind correction factor of 1.2 produced the optimum result and is used for numerical experiments in this study. See the Supplementary Information for the evaluation results of meteorological forcing.

The ERA-20C products describe the spatio-temporal evolution of the atmosphere (on 91 vertical levels, between the surface and 1 Pa), the land-surface (on 4 soil layers), and the ocean waves (on 25 frequencies and 12 directions) by using a coupled atmosphere/land-surface/ocean waves model to reanalyze the weather by assimilating surface observations. The horizontal resolution is approximately 125 km (spectral truncation T159). The temporal resolution of the daily products is 3-hourly. Figure 1 shows the reconstructed 10 m winds and air pressure fields by spatially interpolating from ERA-20C data for January 31–February 1, 1953. The track of the 1953 storm and wind distributions well coincide with the description of the meteorological condition in Section 2. In Schneider et al. (2013), they compared the twentieth century reanalysis data, such as ERA-20C, 20CR (Compo

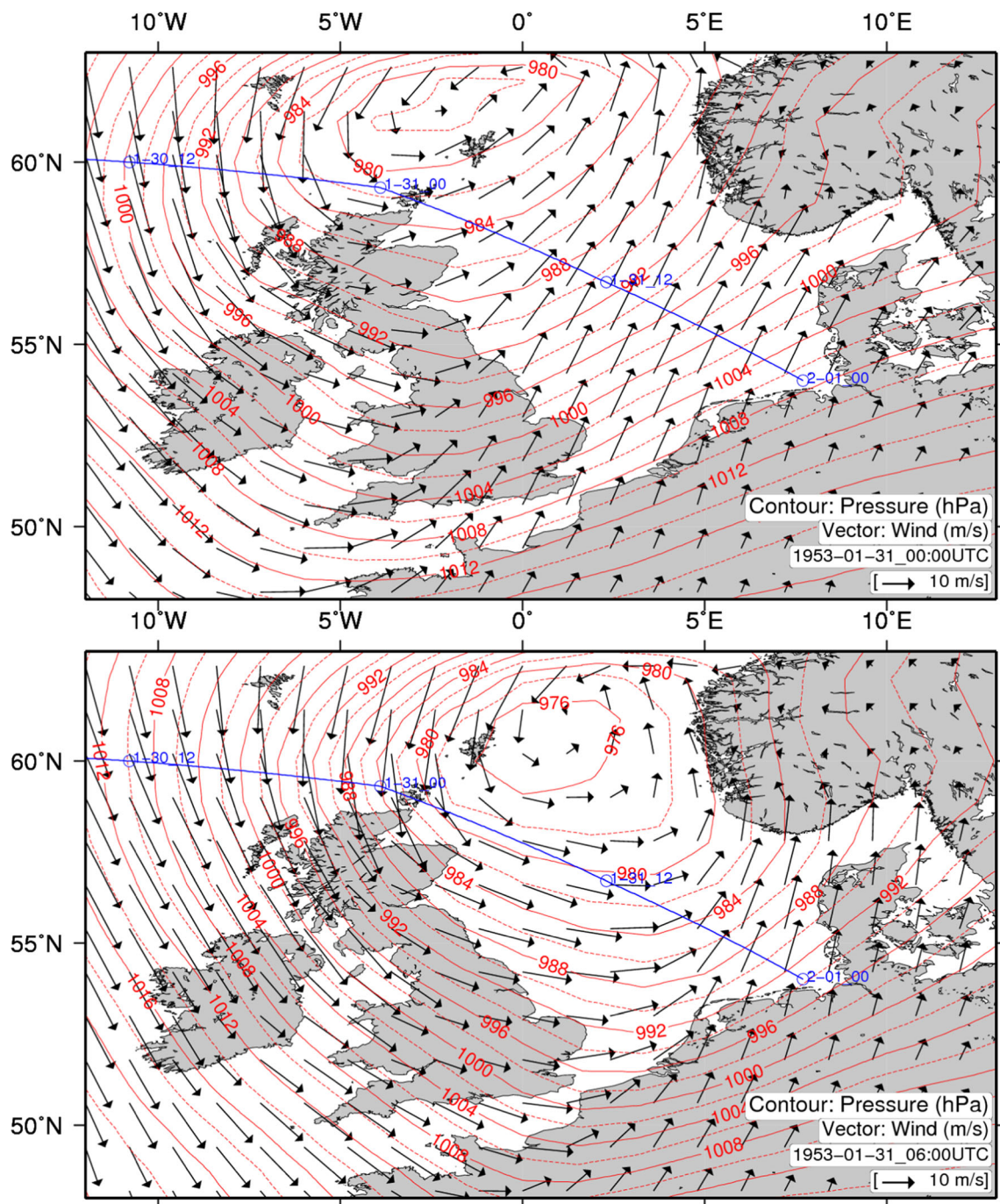


Fig. 1 Winds at 10 m and surface pressure fields from the ERA-20C reanalysis at every 6 h from 00:00 UTC January 31 to 06:00 UTC February 1, 1953 of the 1953 North Sea storm. The format in time is mm-dd_hh

et al. 2011) and NCEP/NCAR reanalysis, with historical chart and other data set, and also concluded that the reanalysis of ERA-20C and 20CR showed in good agreement with other data set and with previous meteorological interpretations of the event.

Figure 3 illustrates the comparison of ERA-20C reanalysis winds with a correction factor of 1.2 and observed winds at the three light vessels. At Dowsing, the ERA-20C winds slightly overestimate compared to the observations, but the reanalysis

winds are in good agreement with the wind observations. In particular, the reanalysis wind at Galloper LV is in quite good agreement with the observation.

3.2 Numerical models

Coupled process-based dynamic models are now widely utilized in earth system science for climate and natural hazards related study. Lee et al. (2013) summarized the

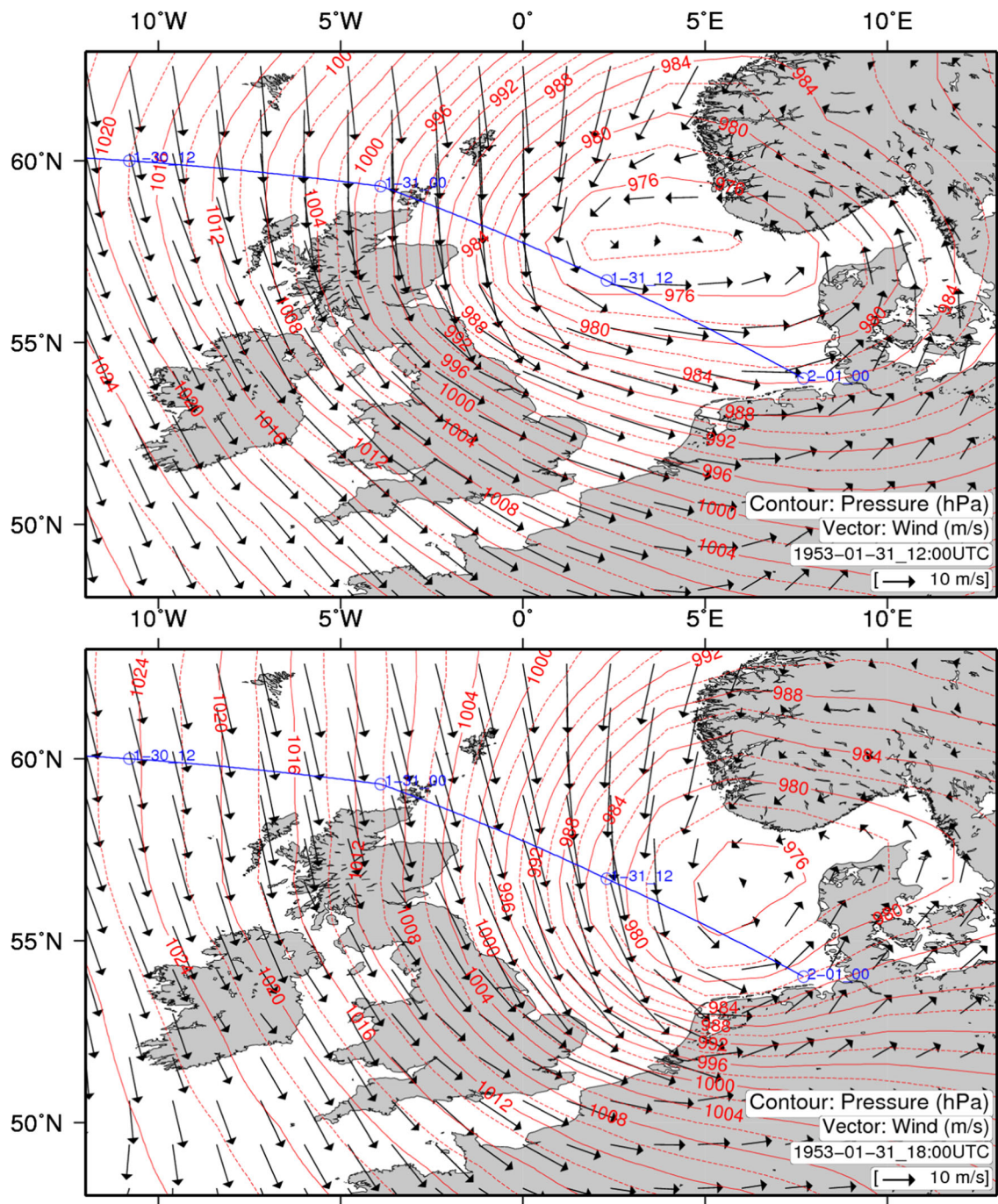


Fig. 1 (continued)

coupled models used in storm surge and storm wave simulations and introduced a new parameterization for the role of surface waves in the storm surge process through whitecapping in deep and depth-induced wave breaking in shallow water.

In this study, ADCIRC (the Advanced CIRCulation model) is adopted for calculating tide and surge. ADCIRC is a continuous-Galerkin, finite-element, shallow-water model that solves the depth-integrated barotropic shallow-water

equations to compute water levels and currents at a range of scales (Atkinson et al. 2004; Dawson et al. 2006; Luettich and Westerink 2004; Westerink et al. 2008). The details of this solution have been published widely (<http://www.nd.edu/~adcirc/manual.htm> to see User’s Manual and Theory Report) and will not be stated here.

For the wave fields, SWAN (Simulating Waves Nearshore) is used to predict the evolution in geographical space and time of the wave action density spectrum, with relative frequency

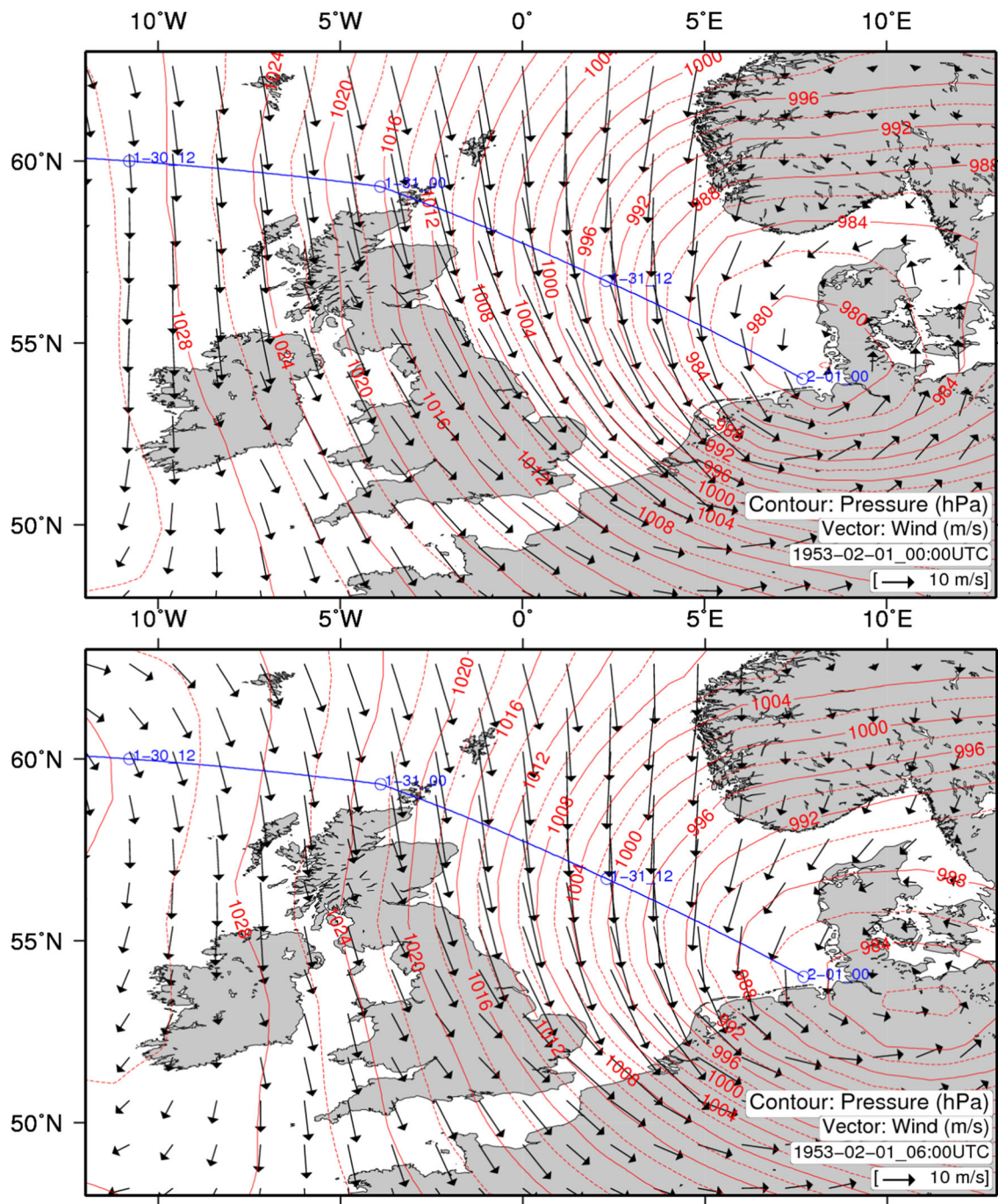


Fig. 1 (continued)

(σ) and wave direction (θ), as governed by the action balance equation (Booij et al. 1999):

$$\frac{\partial N}{\partial t} + \nabla_{\vec{x}} \left[\left(\vec{c}_g + \vec{U} \right) N \right] + \frac{\partial c_{\theta} N}{\partial \theta} + \frac{\partial c_{\sigma} N}{\partial \sigma} = \frac{S_{tot}}{\sigma} \quad (1)$$

The terms on the left-hand side represent, respectively, the change in wave action in time, t , the propagation of wave action in space (with $\nabla_{\vec{x}}$ the gradient operator in geographic

space, the \vec{c}_g wave group velocity, and \vec{U} the ambient current vector), depth and current induced refraction and approximate diffraction (with propagation velocity or turning rate c_{θ}), and the shifting of wave action due to variations in the mean current and depth (with propagation velocity or shifting rate c_{σ}). The source term, S_{tot} , represents wave growth by wind, action lost due to whitecapping, surf breaking and bottom friction, and action exchanged between spectral components in deep and shallow water due to nonlinear effects. The associated

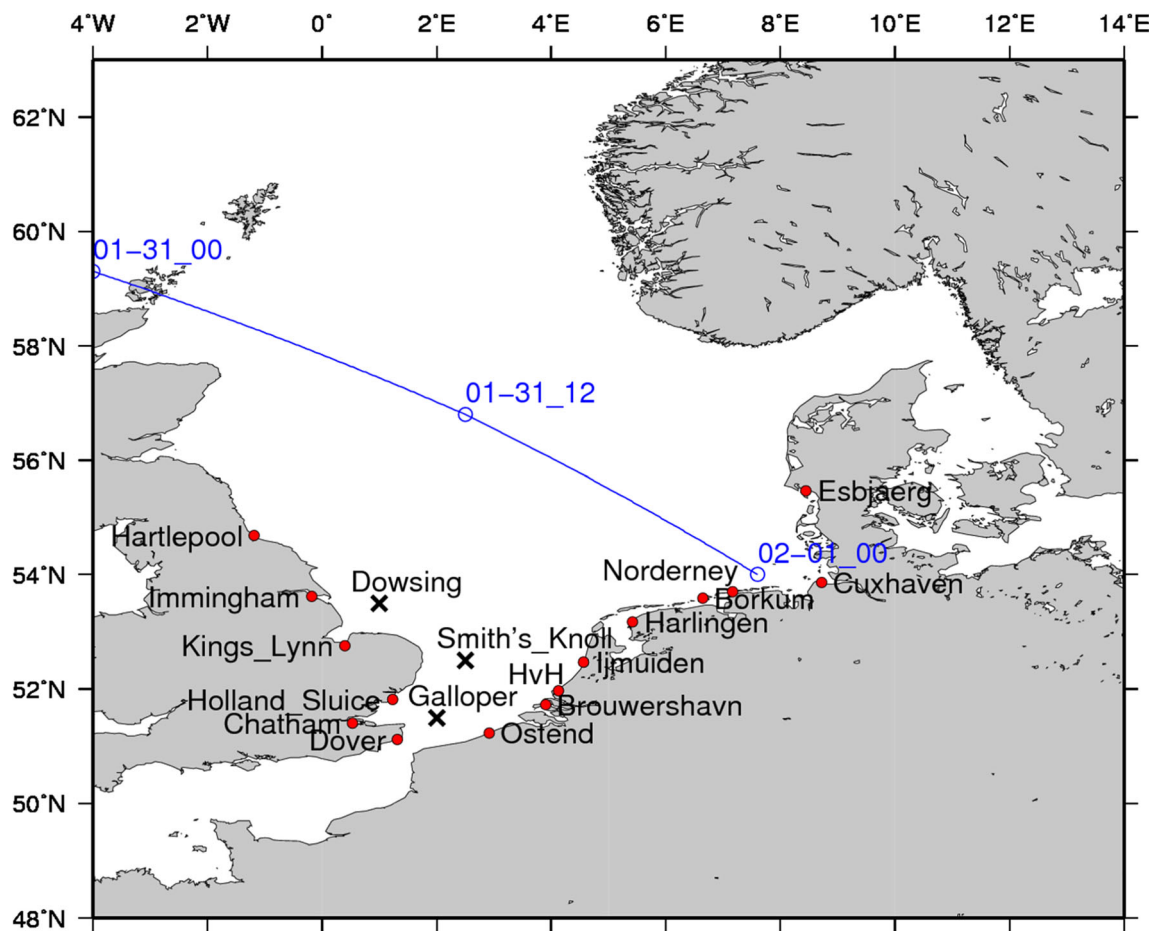


Fig. 2 Tide gauge locations (red circles) along the southern North Sea coast and the estimated track (blue line and circles) of the 1953 North Sea storm referred from Rossiter (1954). Black crosses are locations of three

light vessels. HvH indicates Hoek von Holland in the Netherlands. The format in time is mm-dd_hh

SWAN parameterizations are given by Booij et al. (1999), with all subsequent modifications as presented in version 40.72, including phase-decoupled refraction-diffraction (Holthuijsen et al. 2003), although diffraction is not enabled for the present simulations. SWAN used the unstructured mesh grid system employing an analog to the four-direction Gauss-Seidel iteration technique, and it maintains SWAN’s unconditional stability (Zijlema 2010). SWAN computes the wave action density spectrum at the vertices of an unstructured triangular mesh, and it orders the mesh vertices so that it can sweep through them and update the action density using information from neighboring vertices.

3.3 Model configurations

The computation domain for ADCIRC and SWAN consists of 139,887 nodes and 270,743 elements, and mean, minimum, and maximum node intervals are approximately 5 km, 43 m near-shore, and 36 km near open boundary, respectively. Both use the identical domain allowing the direct communication between two models. Meteorological forcing inputs such as 10 m winds

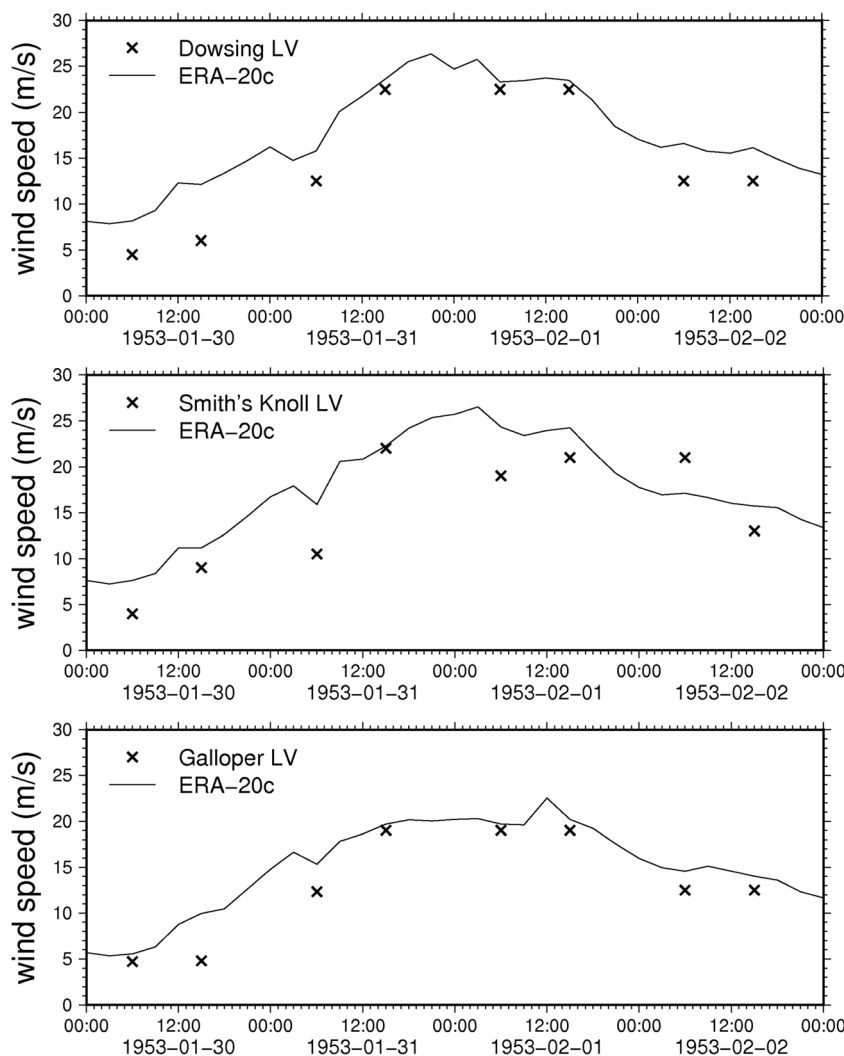
and surface pressure for the period, January 27–February 3, 1953, are prepared from the ERA-20C reanalysis dataset.

With respect to the SWAN model setups for storm waves, the frequency increment factor (X_{ω}), the first frequency (ω_0), the number of frequencies, and the directions for all of the simulations are set as 1.1, 0.031384 Hz, 31, and 36, respectively. The initial spectral densities of 0 is applied in the SWAN simulations. The hybrid bottom friction relationship is used to specify a varying bottom friction coefficient depending on water depth in tide and surge modeling (Luettich and Westerink 2004). The bottom friction coefficient is calculated from a quadratic bottom friction law in deep water, whereas the friction coefficient increases with decreasing depth in shallow water.

3.4 Simulation procedures

SWAN was used for wave computations and ADCIRC was used for tide and surge simulations, and a schematic diagram of the communication between the two models can be found in Choi et al. (2013). The basic structure of this coupling system was developed by Dietrich et al. (2010).

Fig. 3 Comparison of model and observed wind speed. ERA-20c is the model wind from the ERA-20C reanalysis data with a constant correction factor of 1.2 applied. Dowsing LV, Smith’s Knoll LV, and Galloper LV are observations at the named light vessels (see Fig. 2 for locations)



SWAN is driven by wind speeds, water levels, and currents computed at the vertices by ADCIRC. ADCIRC can accept marine winds in various formats, which are adjusted directionally to account for surface roughness (Bunya et al. 2010). Wind is calculated at the vertices through interpolating spatially and temporally with ADCIRC, and then, the results are passed to SWAN. Similarly, the water levels and ambient currents are computed in ADCIRC before being sent to SWAN, where they are used to re-compute the water depth and all relevant wave processes (wave propagation, depth-induced breaking, etc.).

The ADCIRC model is driven partially by radiation stress gradients computed using information from SWAN. These gradients, τ_s , waves are computed by:

$$\tau_{sx,wave} = -\frac{\partial S_{xx}}{\partial x} - \frac{\partial S_{xy}}{\partial y} \tag{2}$$

$$\tau_{sy,wave} = -\frac{\partial S_{xy}}{\partial x} - \frac{\partial S_{yy}}{\partial y} \tag{3}$$

where S_{xx} , S_{xy} , and S_{yy} are the wave radiation stresses (Battjes 1972; Longuet-Higgins and Stewart 1964). The simulation system was designed to cover broad area in scope and size yet providing high degree of resolution in nearshore area.

Approximate mesh sizes in region of interest were formulated as a few tens of meters enabled detailed evaluation of tide and surges in coastal zones with high tidal ranges. Parallel computations of the base model decomposition strategy have been employed.

ADCIRC and SWAN run in series on the same local mesh and core. These two models “leap frog” through time, and each model is forced by information from the other model (Dietrich et al. 2010). SWAN employs a sweeping method to update the wave information at the computational vertices. Therefore, SWAN can take much larger time steps than ADCIRC, which has diffusion- and Courant-time step limitations due to its semi-explicit formulation and its wetting and drying algorithm. Consequently, the coupling interval is designed to be the same as the time step used for SWAN.

Table 1 Summary of tidal harmonic constants comparison in terms of root mean square error (RMSE) between the calculated by ADCIRC and the observed at 7 tidal stations located in the computation domain. The

comparisons with other two tide models are also shown for reference. See Supplementary Information for the locations of tidal stations and scatter diagram for comparison

Tides	ADCIRC RMSE		FEM2004 RMSE		NAO99 RMSE	
	Amp. (cm)	Phase (°)	Amp. (cm)	Phase (°)	Amp. (cm)	Phase (°)
M ₂	15.85	18.25	10.03	19.56	12.75	15.6
S ₂	5.78	18.90	5.16	27.33	5.14	20.13
K ₂	3.29	26.91	2.64	47.75	1.27	34.99
N ₂	4.00	22.51	3.4	28.82	2.81	26.63
K ₁	3.03	61.25	1.31	70.37	3.1	56.41
O ₁	1.30	53.61	0.85	33.56	2.03	42.26
P ₁	1.20	45.62	0.6	80.31	0.92	58.64
Q ₁	0.79	43.13	0.59	40.81	0.73	44.85

As for the coupling between ADCIRC and SWAN, it is assumed that the wave properties are influenced by circulation in the nearshore and the coastal floodplain; thus, ADCIRC runs first on the single coupling interval.

The coupling procedures between the two models are described as follows. Focus is placed on the single coupling interval, which is the same as the time step of SWAN mentioned above. At the beginning of a coupling interval, ADCIRC can be driven partly by the radiation stress gradients computed by SWAN at times corresponding to the beginning and end of the previous interval. ADCIRC uses that information by extrapolating the gradients of the previous coupling interval at all of the time steps in the current coupling interval. When the ADCIRC run is complete, the SWAN run is performed for one time step. At this time, SWAN takes the information from ADCIRC at the same time as ADCIRC. As mentioned above, this information includes wind speeds, water levels, and currents computed by ADCIRC at times corresponding to the beginning and end of the current coupling interval. These variables are averaged for the current one

coupling interval, i.e., a single SWAN time step, and are used as forcing for SWAN at each time step.

To summarize the information shared and coupling of the two models in the above, ADCIRC uses the radiation stress gradients from SWAN, which is always extrapolated forward in time, whereas SWAN uses the wind speeds, water levels, and currents from ADCIRC, which are always averaged to agree with a single SWAN time step.

3.5 Validation of tides

The prescribed tidal forcing of 8 constituents (M₂, S₂, K₁, O₁, N₂, K₂, P₁, and Q₁) is applied at the lateral open ocean boundaries from the National Astronomical Observatory’s (NAO) ocean tide model (Matsumoto et al. 2000). For the storm surge simulations, the barotropic ocean states are considered such that the influences of the temperature and salinity profiles in the ocean remain uniform. The bathymetry for the wave and storm surge simulations is taken from the GEBCO 30 arc-sec database (IOC et al. 2003). The tide-only simulation of

Table 2 Numerical experiments, descriptions, and conditions

Run	Tide	Surge	Wave	Description	Conditions
T	○	×	×	Tide only	1. Tides at open boundaries: M ₂ , S ₂ , K ₁ , O ₁ , N ₂ , K ₂ , P ₁ , and Q ₁ 2. Atmospheric forcing: 10 m winds and surface pressure from ERA-20C reanalysis 3. Varying bottom friction coefficient depending on water depth 4. Simulation period: 00:00 27th of January~00:00 3rd of February 1953
S	×	○	×	Surge by atmospheric forces	
W	×	×	○	Wave only	
TS	○	○	×	Surge by atmospheric forces and tide	
TSW	○	○	○	Surge by atmospheric forces, tide, and wave effects	
TSW-T	–	–	–	Difference between TSW and T	
TS-T	–	–	–	Difference between TS and T	
TSW-W	–	–	–	Difference between TSW and W	
TSW-TS	–	–	–	Difference between TSW and TS	

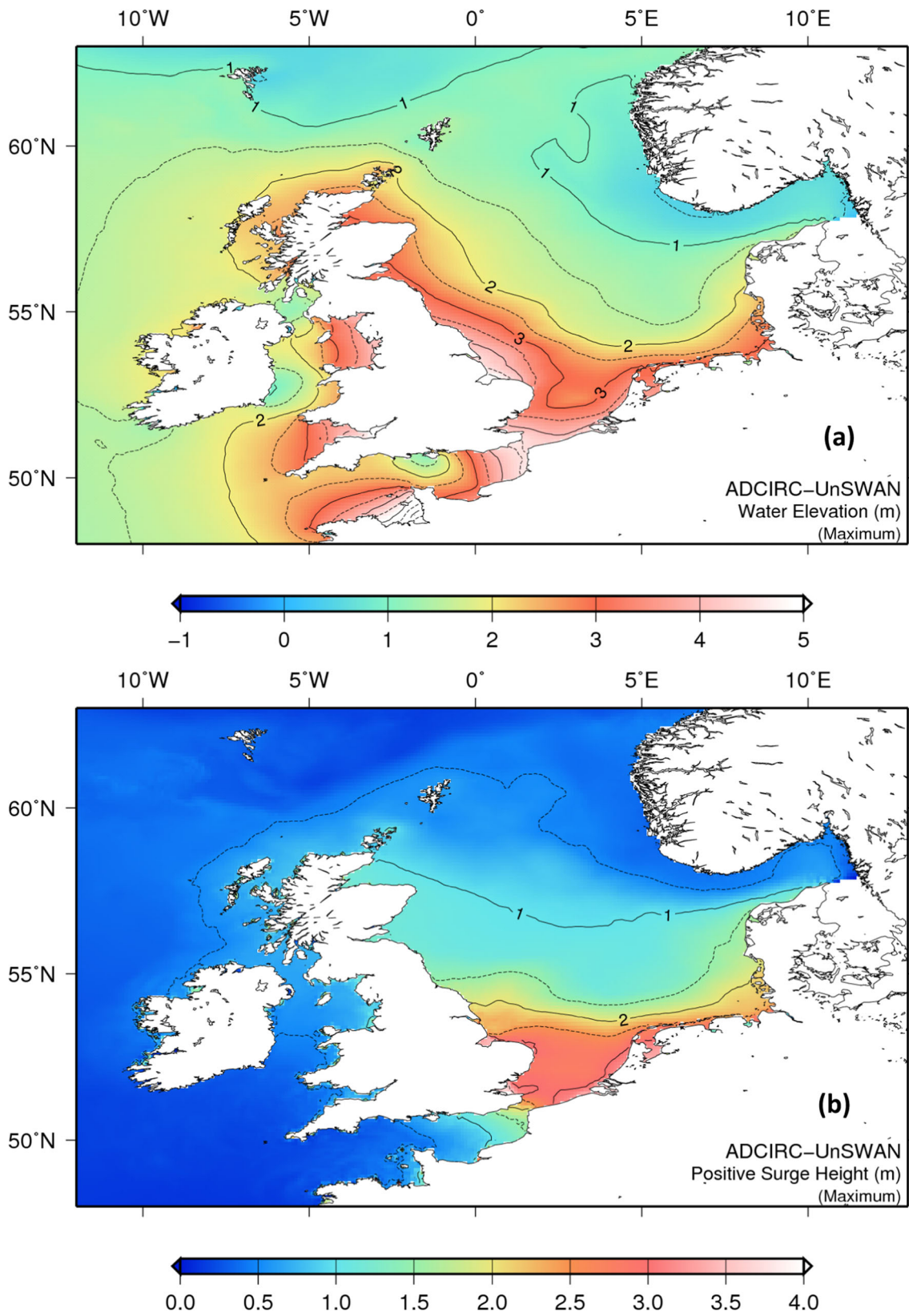


Fig. 4 **a** Maximum calculated water levels from the TSW run and **b** maximum calculated surge heights obtained from TSW-T experiment over the simulation period in the North Sea

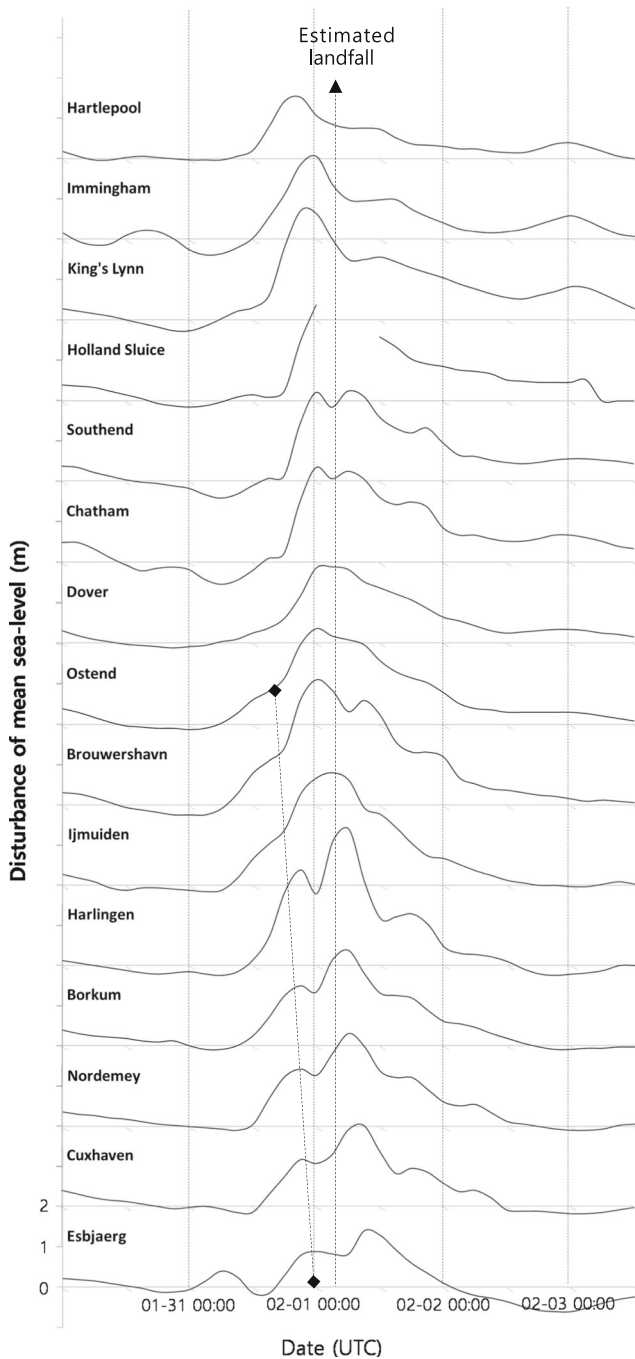


Fig. 5 Mean sea-level disturbances due to the 1953 North Sea storm reproduced from the Table 3 of Rossiter (1954)

ADICRC model is first carried out for 65 days including a spring-neap cycle and a harmonic analysis was performed with the last 60 days results. Then the harmonic constants for amplitude and phase of the 8 tidal constituents are compared with the observed harmonic constants at 7 tidal stations located within the computational domain. Moreover, the computed harmonic constants by ADCIRC are also compared

with those obtained from other tide models such as FES2004 (Lyard et al. 2006) and NAO99 (Matsumoto et al. 2000). Table 1 depicts the comparison results in terms of root mean square error (RMSE), illustrating that the model performs reasonably well. In addition, the computed tidal charts for amplitude and phase are also compared with those from a previous study by Howarth (1990) (see also Supplementary Information for the locations of tidal stations, coefficient of determination and scatter diagram for validation of tides in the North Sea). The validation results of storm surge and waves are described in detail in Sections 4.1 and 4.2, respectively.

3.6 Numerical experiments

A set of numerical experiments are performed to model the 1953 North Sea storm surge including the effects of waves on storm surge. Table 2 presents the summary of numerical experiments with different forcing conditions. First, the tide (T), surge (S), and wave (W) simulations are carried out independently with meteorological forcing such as 10 m winds and surface pressure from the ERA-20C reanalysis for surge and wave modeling. Then, surge modeling is conducted with the coupled model forced by the 10 m winds, surface pressure, tide, and waves (TSW). To investigate the effects of waves on storm surge, an additional surge modeling without wave coupling (TS) is also carried out.

4 Results and discussion

4.1 Storm surge

Figure 4a illustrates the spatial distribution of computed maximum water levels due to tide, wind, and pressure forcings, and the effects of waves from the TSW run for the simulation period in the North Sea. In the interpretations of simulation results, the east coast of the UK, the German Bight, and the low-lying coast of the Netherlands are highlighted hereinafter. The maximum water level from the TSW run in the low-lying Dutch delta area is about 3.5 m near the inlets and even higher in the river mouths. The maximum water levels along the east coast of the UK including the Essex are about 4 m and over 5 m in The Wash. In the German Bight, the maximum water level is approximately 3.0 m and even higher near Cuxhaven.

Figure 4b shows spatial distribution of calculated maximum surge heights due to wind and pressure forcings and the effects of waves obtained from the TSW-T experiment in the North Sea. The maximum surges gradually increase from about 1 m in the north to more than 3 m in the south of the east coast of the UK. Large maximum surges are found in The Wash and Thames estuary of the UK of approximately

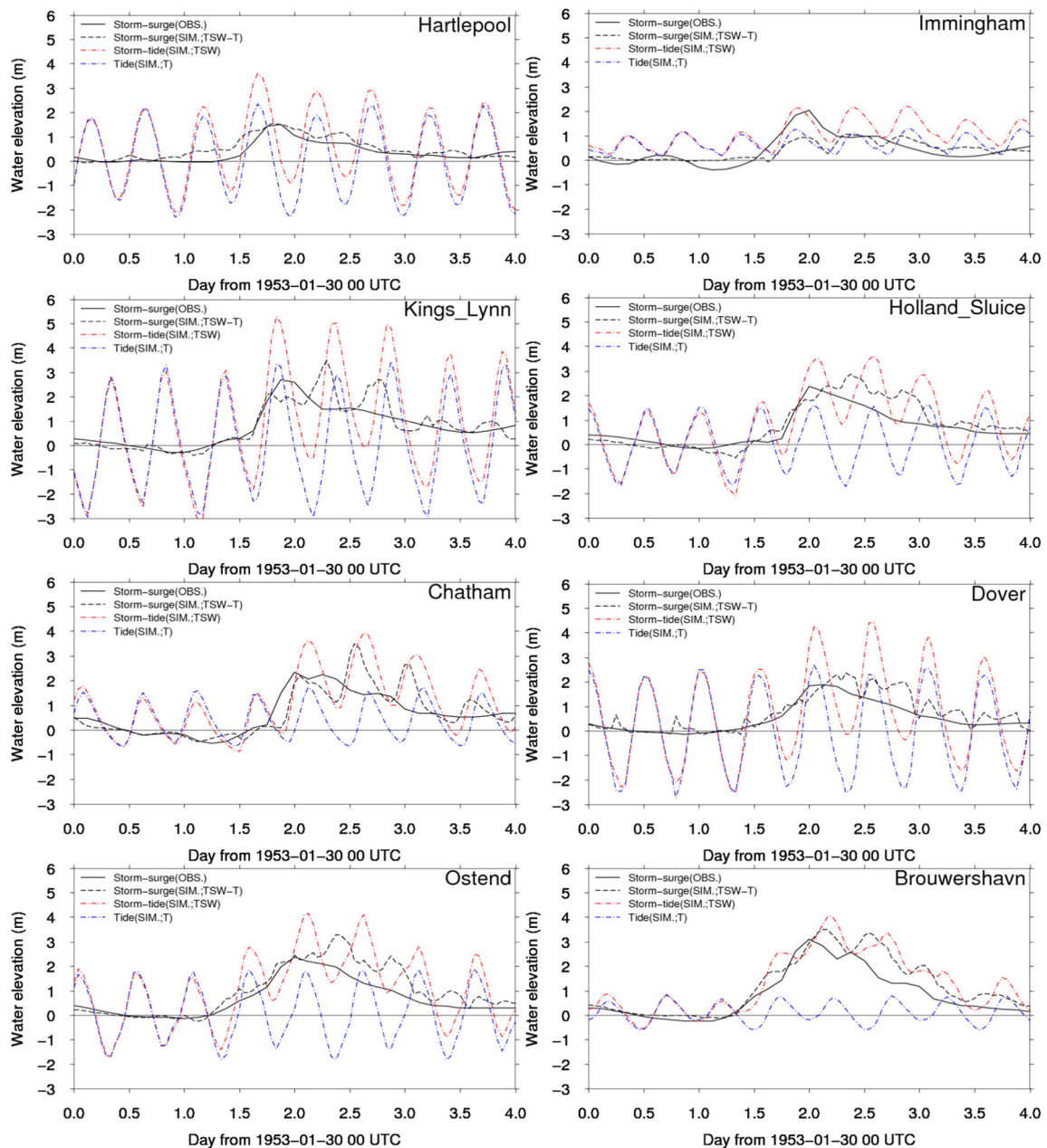


Fig. 6 Comparisons between the observed and the calculated storm surges along the southern coast of the North Sea

3.5 m, in the low-lying coast of the Netherlands more than 3 m, and in the shallow coastal zones in German Bight more than 2.5 m. The spatial pattern of maximum surges in the southern North Sea agrees well with that of Wolf and Flather (2005) and De Ronde and Gerritsen (1989). However, the maximum surges are slightly higher than those of two studies. The maximum surges in the Dutch delta areas are more than 3 m near the inlets and higher along the upstream. In the German Bight, the maximum surges are approximately 2.5 m, and 3 m near Cuxhaven and along the river mouth of Elbe River.

To validate the computed surge heights, hourly water level records along the southern coast of the North Sea are collected

from Rossiter (1954) and used for comparison. It contains not only the tidal records in the UK but those in other countries adjacent to the North Sea. It should be also noted that at some locations, the storm surges are reconstructed by temporally and spatially interpolating its own and nearest available records, and the storm surges are prepared for the study of wind effects and do not represent the true surge since local barometric effects are removed. Figure 5 depicts the observed surge heights obtained from Rossiter (1954). The peaks of hourly tide records are ranging from 2 to 3.5 m. The highest storm surge of 3.31 m is found at Harlingen in the Netherlands. Then, the observed surge heights are compared with computed results from the TSW-T experiment.

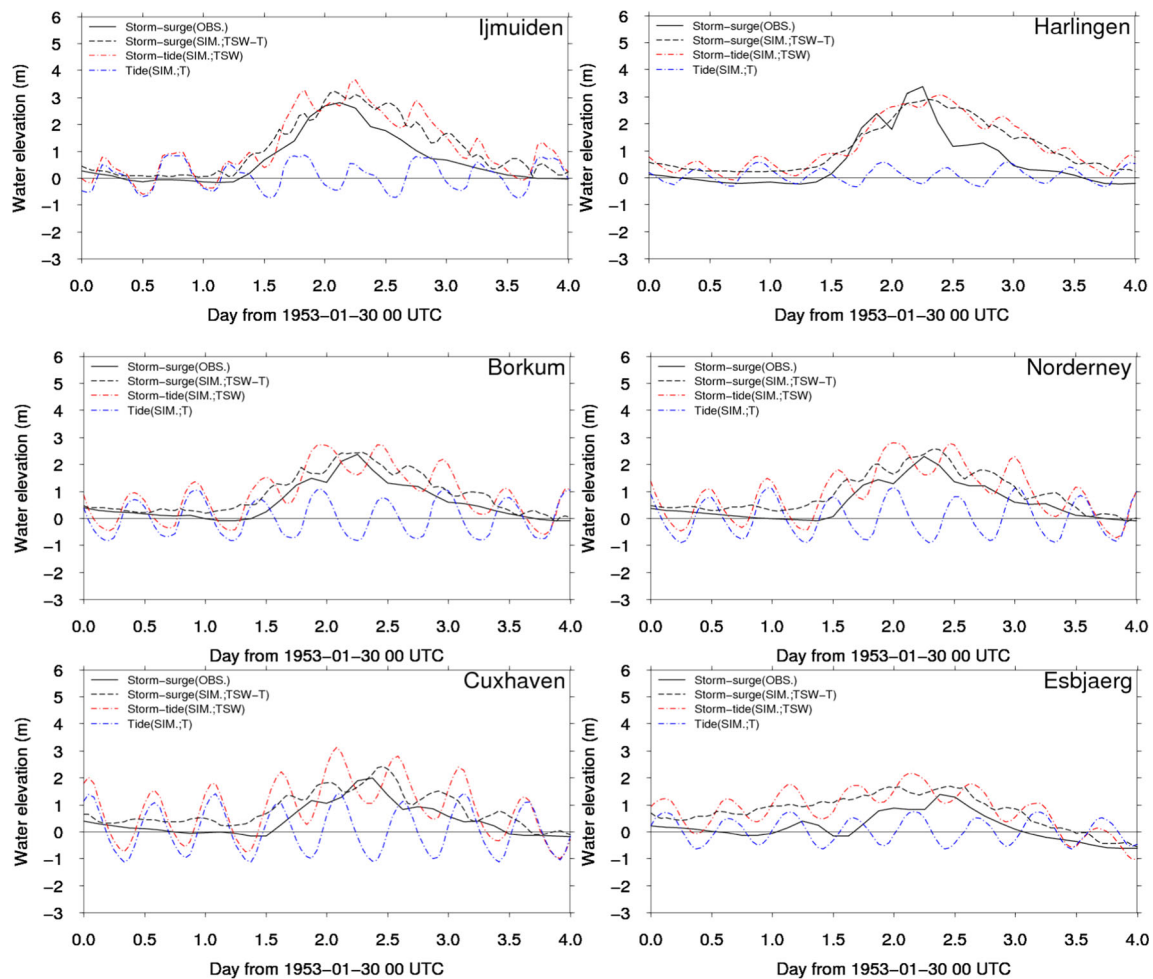


Fig. 6 (continued)

In Fig. 6, the comparisons of surge heights are presented from the east coast of the UK and the Dutch delta area to the coast of German Bight in anticlockwise direction. The peak of the storm surge at Hartlepool is appeared about 18:00 UTC January 31 and then the peaks of storm surges are appeared in order from the north to Dover strait at Dover at approximately 00:00 UTC February 1. The simulated peaks of storm surges are slightly overestimated in general, but the occurrence times are generally captured well. Wolf and Flather (2005) compared their computed surge elevations with tide gauge data that is different and higher than those of Rossiter (1954).

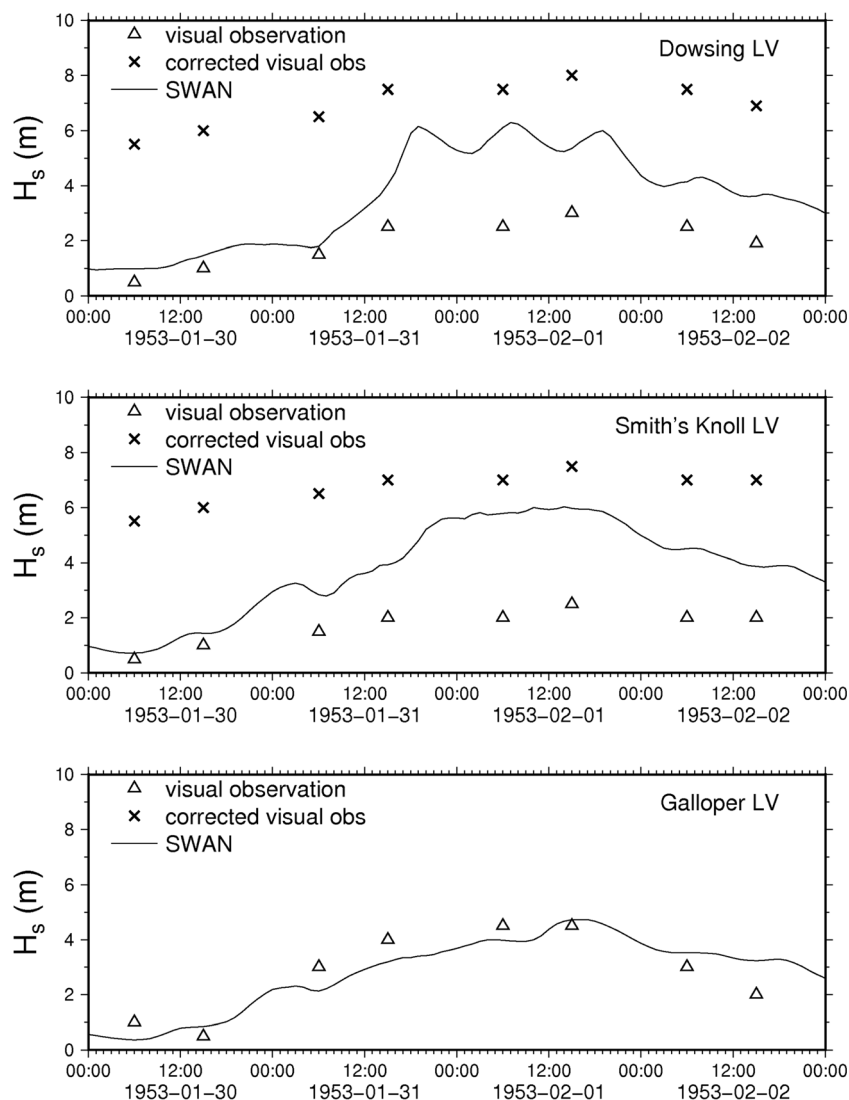
Along the southern coast of the North Sea, the peaks of the storm surges are observed in anticlockwise order approximately from 00:00 February 1 at Ostend to 10:00 February 1 at Esbjaerg as shown in Figs. 5 and 6. From Ostend to Harlingen, the computed storm surges are slightly overestimated but temporal changes of surge elevations are well captured. At Borkum, Norderney, and Cuxhaven, the observed surge elevations are also slightly higher, and the computed storm surges are over 2 m and grow earlier than the observed ones.

In German literature, Küstenausschuss Nord- und Ostsee (1969) and Jensen et al. (2011), a much higher maximum wind surge at Hoek van Holland (HvH in Fig. 2) of 3.28 m is reported between Brouwershavn and IJmuiden. The calculated storm surge peaks at Brouwershavn and IJmuiden are 3.5 and 3.25 m, while the observed surges are 3.1 and 2.8 m. Therefore, the computed storm surges in this study are in quite good agreement with the observations and thought to be very reasonable. Since the surge elevations from Rossiter (1954) do not take into account the barometric effects, and the observed tide gauge records from Wolf and Flather (2005) and Küstenausschuss Nord- und Ostsee (1969) are higher than those of Rossiter’s data, it can be deduced that the Rossiter’s data are not complete and underestimated.

4.2 Storm waves

Figure 7 exhibits the time series of wave heights at the locations of three light vessels off the east coast of the UK. It seems probable that the maximum observed significant wave heights at Dowsing and Smith’s Knoll are underestimated,

Fig. 7 Comparison of model and observed significant wave heights at the locations of light vessels



possibly owing to the ambiguity introduced by the method of recording visual observations (Wolf and Flather 2005). It should be also noted that the maximum significant wave height of 2.5 m at Smith's Knoll does not agree with reports of wave crests over 20 ft (6 m) high (Lawford 1954). According to Wolf and Flather (2005), it seems plausible that at least the wave heights on February 1 were misreported. The maximum calculated significant wave heights at Dowsing and Smith's Knoll in Fig. 8 are over 6 m and lower than the corrected visual observations.

Figure 8 presents spatial distributions of maximum calculated significant wave heights for the simulation period and the calculated mean wave period in the North Sea from the W experiment. The significant wave heights in the north-south fetch of the North Sea are high over 10 m, while those along

the southern North Sea are approximately 6 m. Near the inlets and bays in the southern North Sea, it gradually decreases down to 2–3 m. In the German Bight, the east coast of the UK and the delta area of the Netherlands, waves are calculated approximately 3–4 m along the coast and inlets. The spatial distribution of wave heights represents the complex geometric features well along the coastline, implying the importance of the model resolution along the coast in shallow water.

The computed mean wave period is approximately 9 s in the northern and central North Sea, whereas the peak wave period is approximately 12 s. In the southern North Sea, the mean wave period is about 7 s gradually decreasing down below 6 s along the coast and inlets, while the peak wave period is about 8 s in the southern North Sea.

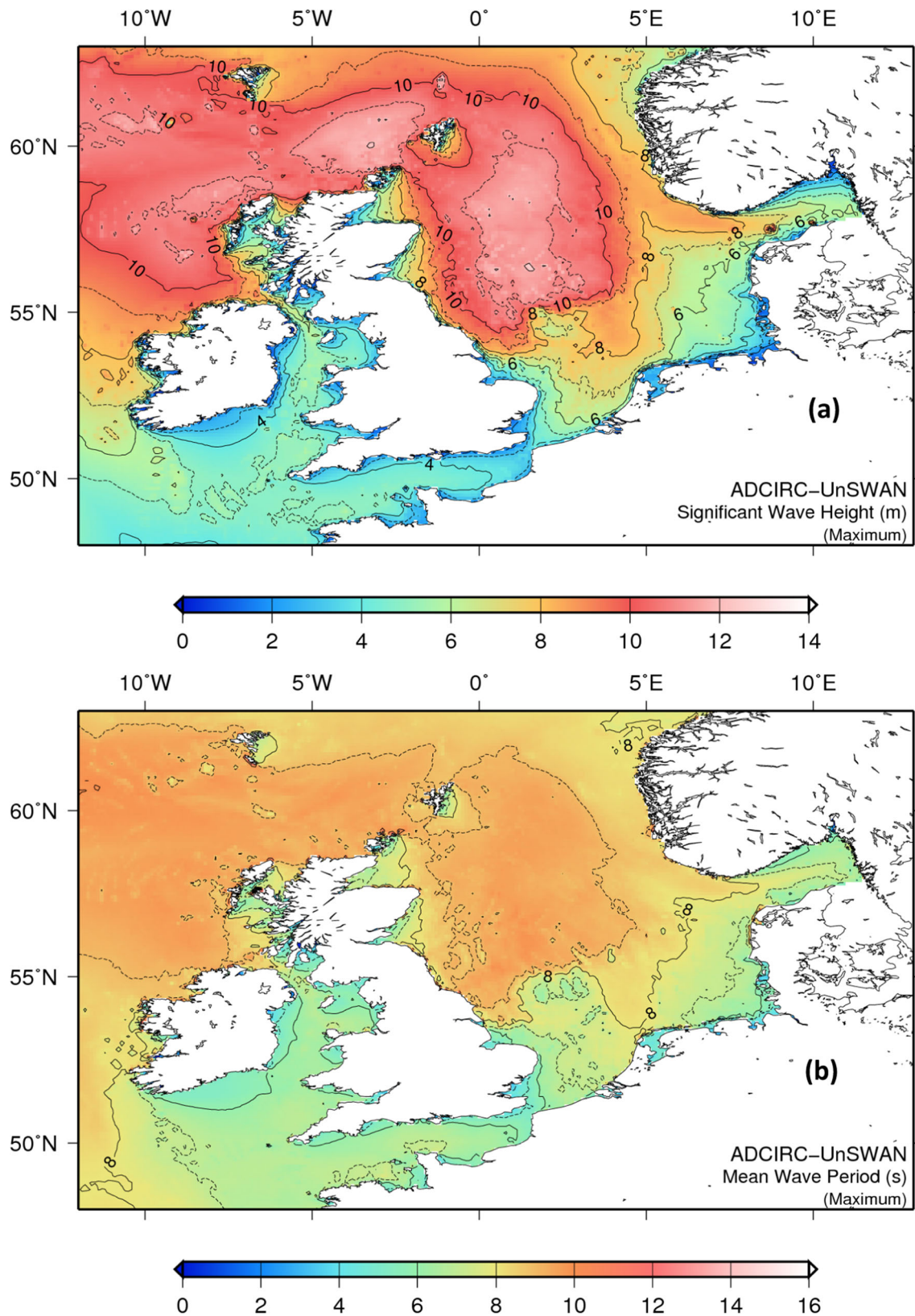


Fig. 8 a Calculated maximum significant wave heights and b calculated mean wave period over the simulation period in the North Sea from the W run

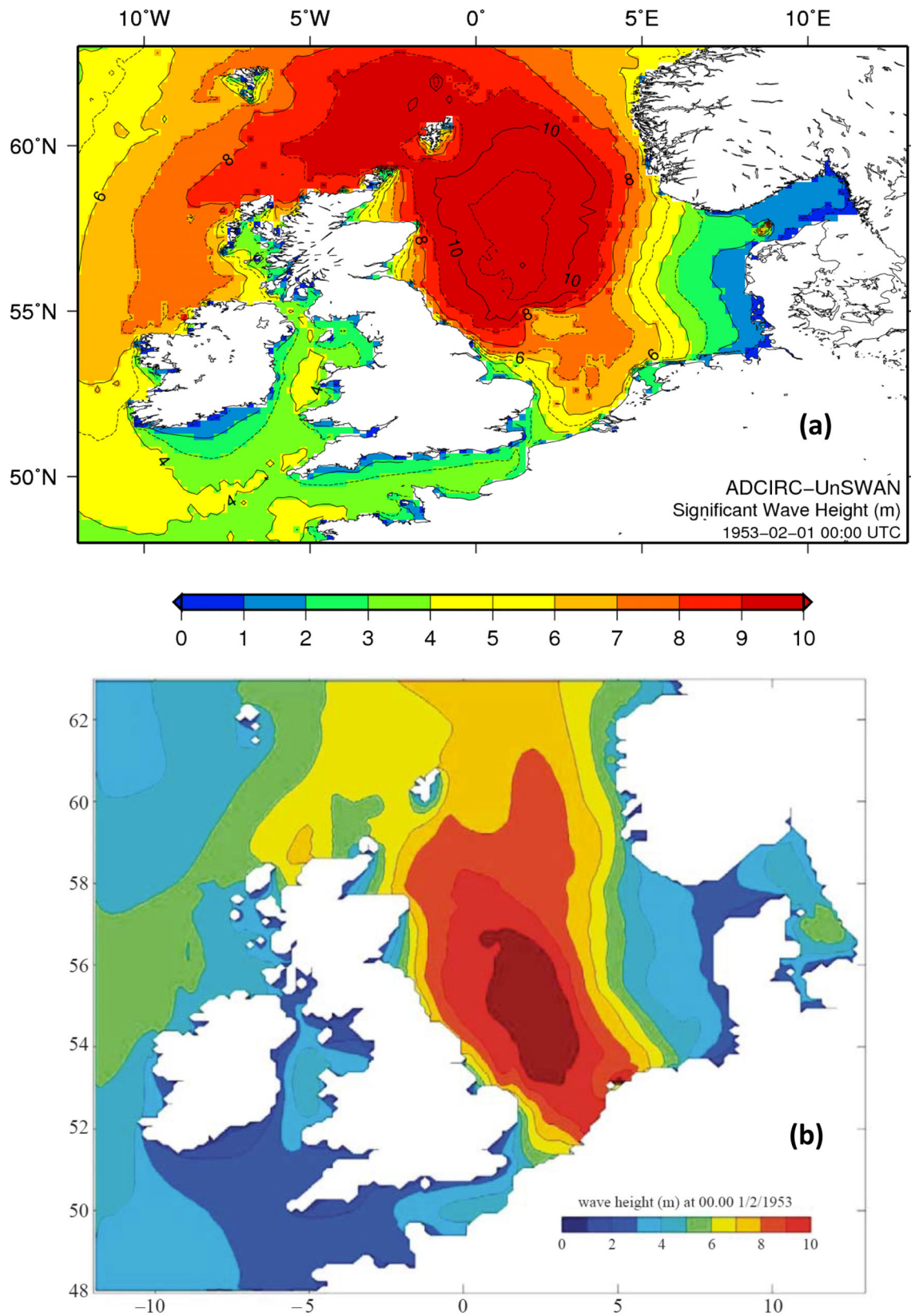


Fig. 9 Comparison of **a** calculated significant wave height obtained from W run of this study and **b** calculated significant wave height by Wolf and Flather (2005) in the North Sea at 00:00 UTC February 1, 1953

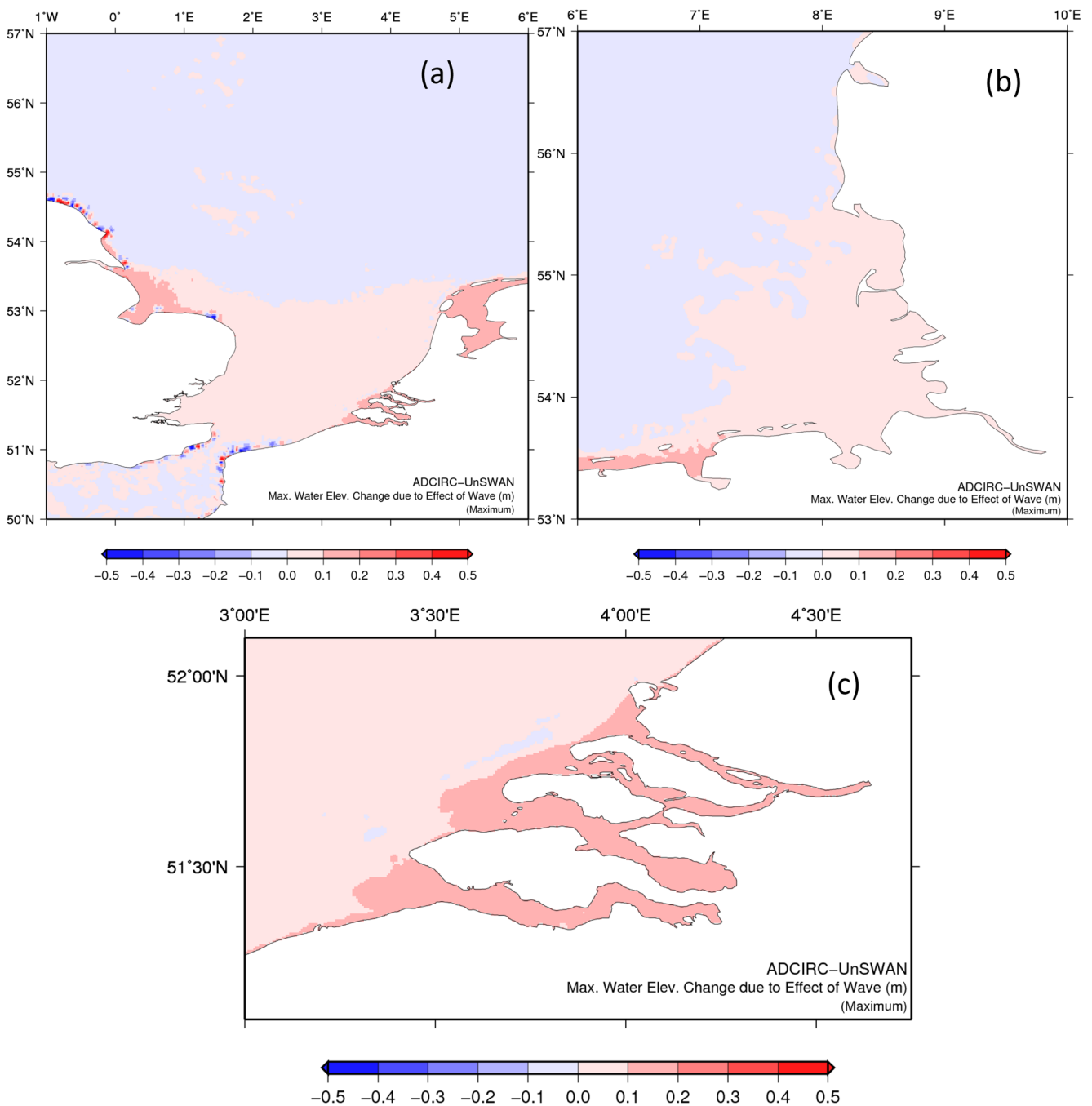


Fig. 10 Differences of calculated maximum water levels between TSW and TS experiments over the simulation period, depicting the effects of waves on water levels for **a** the UK east coast and the southern North Sea, **b** the German Bight, and **c** the Dutch delta areas

The computed significant wave height at 00:00 UTC February 1, 1953 and that from Wolf and Flather (2005) at the same time are compared in Fig. 9. The significant wave height in the central North Sea is over 11 m in this study, while that from Wolf and Flather (2005) is higher than 10 m. However, in the northern North Sea, the significant wave heights are approximately 10 m and 9 m, respectively. In the

southern North Sea along the low-lying delta area of the Netherlands, the significant wave height of this study gradually decreases below 6 m, while that from Wolf and Flather (2005) is remained high over 8 m. It is thought to be partly due to relatively low resolution of storm surge and wave models and incorrect bathymetry. In particular, the effect of Dogger Bank in the south-central North Sea is not appeared in the

significant wave height of Wolf and Flather (2005) result, assuming no significant changes in bathymetry. Therefore, the significant wave height of Wolf and Flather (2005) in the southern North Sea in Fig. 9b remains high close to the low-lying coast of the Netherlands, whereas the significant wave height of this study in Fig. 9a gradually decreases in the southern North Sea.

In Wolf and Flather (2005), wave measurement data at three light vessels, named Dowsing, Smith's Knoll, and Galloper in order from the north, off the southern east coast of the UK, are presented in Fig. 7. They are based on visual observations and the maximum values of corrected visual observed significant wave heights at Dowsing, Smith's Knoll, and Galloper between January 30 and February 3, 1953 are approximately 8 m, 7.5 m, and 4.5 m, respectively. The maximum calculated significant wave heights at the same locations are approximately 6.3 m, 6.0 m, and 4.7 m, respectively. It seems that the computed significant wave height at Smith's Knoll from Wolf and Flather (2005) is somehow overestimated due to rough resolution and bathymetry.

Moreover, many literatures during this time about this storm surge is probably written in German or Dutch. It is problematic to ignore this literature. In Tomczak (1955), values can be found that the waves during the storm surge with wave height up to 9 m and periods between 8 to 10 s in the northern and central North Sea. At the Dutch coast, wave heights of about 6 to 7 m with approximately the same period. Those records at the Dutch coast agree well with the wave heights and period of this study as in Fig. 8.

4.3 Effects of wave setup

By using the coupled tide-surge-wave model, the effects of waves in water level due to wave setup through the radiation stress gradient can be investigated. In Fig. 10, the differences of maximum calculated water levels between TSW and TS experiments are illustrated, indicating the effects of wave setup on storm surges. Significant positive effects with approximately 0.2 m are observed in The Wash and the delta areas of the Netherlands. It is about 10% of observed maximum storm surges.

5 Conclusions

The 1953 North Sea storm surge is probably one of the most studied severe coastal floods in the history. Several factors led to the devastating storm surge along the southern North Sea coast in combination of strong and sustained northerly winds, invert barometric effect, high spring tide, an accumulation of the large surge in the Strait of Dover, and high storm waves. In this study, the wind and pressure fields are reproduced by using ERA-20C reanalysis data with a constant correction

factor of 1.2 for winds. The reproduced 10 m winds depict a quite good agreement with wind observations at light vessels off the east coast of the UK. Then, we have examined the 1953 North Sea storm surge processes with a coupled tide-surge-wave model. The resulting tides, storm surge, and waves during the 1953 North Sea storm were reproduced and coincided reasonably well with historical records of storm surge and waves, and related literatures.

From the coupled tide, surge, and wave modeling, the result shows that wave setup due to breaking waves play a role in surge heights up to 10% of total storm surge with 0.2 m in limited coastal areas such as The Wash in the UK and the low-lying delta areas in the Netherlands.

The resulting modeling system considering tide, surge, and waves can be used extensively for the prediction of the typhoon surge, wave of extreme conditions, and usual barotropic forecast.

Acknowledgements We thank two anonymous reviewers, whose valuable comments helped us improve the quality of this paper.

Funding information The study was supported by the Grant-in-Aid for Scientific Research (17K06577) from JSPS, Japan, and the project titled 'Study of Air-Sea Interaction and Process of RI Typhoon', funded by the Ministry of Oceans and Fisheries, Korea. The study was also supported by the project entitled 'Solving Grand-challenge Problems in Science and Engineering to Expand Utilization of Supercomputing' at Korea Institute of Science and Technology Information.

References

- Atkinson JH, Westerink JJ, Hervouet JM (2004) Similarities between the quasi-bubble and the generalized wave continuity equation solutions to the shallow water equations. *Int J Numer Methods Fluids* 45:689–714. <https://doi.org/10.1002/flid.700>
- Battjes JA (1972) Radiation stresses in short-crested waves. *J Mar Res* 30: 56–64
- Baxter PJ (2005) The east coast Big Flood, 31 January–1 February 1953: a summary of the human disaster. *Philos Trans R Soc A Math Phys Eng Sci* 363:1293–1312. <https://doi.org/10.1098/rsta.2005.1569>
- Booij N, Ris RC, Holthuijsen LH (1999) A third-generation wave model for coastal regions, 1. Model description and validation. *J Geophys Res* 104:7649–7666
- Bunya S, Dietrich JC, Westerink JJ, Ebersole BA, Smith JM, Atkinson JH, Jensen R, Resio DT, Luettich RA, Dawson C, Cardone VJ, Cox AT, Powell MD, Westerink HJ, Roberts HJ (2010) A high-resolution coupled riverine flow, tide, wind, wind wave, and storm surge model for southern Louisiana and Mississippi. Part I: model development and validation. *Mon Weather Rev* 138:345–377. <https://doi.org/10.1175/2009mwr2906.1>
- Choi B, Min B, Kim K, Yuk J (2013) Wave-tide-surge coupled simulation for typhoon Maemi. *China Ocean Eng* 27:141–158. <https://doi.org/10.1007/s13344-013-0013-0>
- Compo GP, Whitaker JS, Sardeshmukh PD, Matsui N, Allan RJ, Yin X, Gleason BE, Vose RS, Rutledge G, Bessemoulin P, Brönnimann S, Brunet M, Crouthamel RI, Grant AN, Groisman PY, Jones PD, Kruk MC, Kruger AC, Marshall GJ, Mauerer M, Mok HY, Nordli Ø, Ross TF, Trigo RM, Wang XL, Woodruff SD, Worley SJ (2011) The twentieth century reanalysis project. *Q J R Meteorol Soc* 137:1–28. <https://doi.org/10.1002/qj.776>

- Dawson C, Westerink JJ, Feyen JC, Pothina D (2006) Continuous, discontinuous and coupled discontinuous–continuous Galerkin finite element methods for the shallow water equations. *Int J Numer Methods Fluids* 52:63–88. <https://doi.org/10.1002/flid.1156>
- De Ronde JG, Gerritsen H (1989) The 1953 storm simulated with the Dutch Continental Shelf model. Unpublished WL/Delft Hydraulics/Rijkswaterstaat Report Z307 (in Dutch), 51 pp
- Dietrich JC, Bunya S, Westerink JJ, Ebersole BA, Smith JM, Atkinson JH, Jensen R, Resio DT, Luettich RA, Dawson C, Cardone VJ, Cox AT, Powell MD, Westerink HJ, Roberts HJ (2010) A high-resolution coupled riverine flow, tide, wind, wind wave, and storm surge model for southern Louisiana and Mississippi. Part II: synoptic description and analysis of hurricanes Katrina and Rita. *Mon Weather Rev* 138:378–404. <https://doi.org/10.1175/2009mwr2907.1>
- Flather RA (1984) A numerical model investigation of the storm surge of 31 January and 1 February 1953 in the North Sea. *Q J R Meteorol Soc* 110:591–612. <https://doi.org/10.1002/qj.49711046503>
- Gerritsen H (2005) What happened in 1953? The Big Flood in the Netherlands in retrospect. *Philos Trans R Soc A Math Phys Eng Sci* 363:1271–1291
- Hansen W (1956) Theorie zur Errechnung des Wasserstandes und der Strömungen in Randmeeren nebst Anwendungen I. *Tellus* 8:287–300. <https://doi.org/10.1111/j.2153-3490.1956.tb01227.x>
- Hickey KR (2001) The storm of 31 January to 1 February 1953 and its impact on Scotland. *Scott Geogr J* 117:283–295. <https://doi.org/10.1080/00369220118737129>
- Holthuijsen LH, Herman A, Booij N (2003) Phase-decoupled refraction–diffraction for spectral wave models. *Coast Eng* 49:291–305. [https://doi.org/10.1016/S0378-3839\(03\)00065-6](https://doi.org/10.1016/S0378-3839(03)00065-6)
- Howarth MJ (1990) Atlas of tidal elevations and currents around the British Isles. Proudman Oceanography Laboratory, London
- IOC, IHO, BODC (2003) Centenary edition of the GEBCO digital atlas, published on CD-ROM on behalf of the Intergovernmental Oceanographic Commission and the International Hydrographic Organization as part of the General Bathymetric Chart of the Oceans
- Jensen J, Frank T, Wahl T, Dangendorf S (2011) Analyse von hochaufgelösten Tidewasserständen und Ermittlung des MSL an der deutschen Nordseeküste. KFKI-Projekt AMSeL. Universität Siegen, Siegen
- Lawford CAL (1954) Currents in the North Sea during the 1953 gale. *Weather* 9:67–72. <https://doi.org/10.1002/j.1477-8696.1954.tb01742.x>
- Lee HS, Yamashita T, Hsu JRC, Ding F (2013) Integrated modeling of the dynamic meteorological and sea surface conditions during the passage of Typhoon Morakot. *Dyn Atmos Oceans* 59:1–23. <https://doi.org/10.1016/j.dynatmoce.2012.09.002>
- Longuet-Higgins MS, Stewart R (1964) Radiation stresses in water waves; a physical discussion, with applications. *Deep-Sea Res Oceanogr Abstr* 11:529–562. [https://doi.org/10.1016/0011-7471\(64\)90001-4](https://doi.org/10.1016/0011-7471(64)90001-4)
- Luettich R, Westerink J (2004) Formulation and numerical implementation of the 2D/3D ADCIRC. Finite element model version 44.XX
- Lyard F, Lefèvre F, Letellier T, Francis O (2006) Modelling the global ocean tides: modern insights from FES2004. *Ocean Dyn* 56:394–415. <https://doi.org/10.1007/s10236-006-0086-x>
- Matsumoto K, Takanezawa T, Ooe M (2000) Ocean tide models developed by assimilating TOPEX/POSEIDON altimeter data into hydrodynamical model: a global model and a regional model around Japan. *J Oceanogr* 56:567–581
- MetOffice (2014) 1953 East coast flood – 60 years on. doi:<http://www.metoffice.gov.uk/news/in-depth/1953-east-coast-flood>
- Muir Wood R, Drayton M, Berger A, Burgess P, Wright T (2005) Catastrophe loss modelling of storm-surge flood risk in eastern England. *Philos Trans R Soc A Math Phys Eng Sci* 363:1407–1422. <https://doi.org/10.1098/rsta.2005.1575>
- Ostsee KN-U (1969) Zusammenfassung der Untersuchungsergebnisse der ehemaligen Arbeitsgruppe “Sturmfluten” und Empfehlungen für ihre Nutzenanwendung beim Seedeichbau. *Die Küste* 17:Heide, Holstein: Boyens. S. 81–103
- Poli P, Hersbach H, Tan D, Dee D, Thépaut J-N, Simmons A, Peubey C, Laloyaux P, Komori T, Berrisford P, Dragani R, Trémolet Y, Holm E, Bonavita M, Isaksen L, Fisher M (2013) The data assimilation system and initial performance evaluation of the ecmwf pilot reanalysis of the 20th-century assimilating surface observations only (era-20c). ECMWF, Shinfield Park, Reading, p 14
- Rijkswaterstaat, KNMI (1961) Verslag over de stormvloed van 1953 (Report on the 1953 Flood). the Netherlands (In Dutch with English Summary)
- Rossiter JR (1954) The north sea storm surge of 31 January and 1 February 1953. *Philos Trans Royal Soc A* 246:371–400
- Schneider T, Weber H, Franke J, Brönnimann S (2013) The storm surge event of the Netherlands in 1953. In: Brönnimann S, Martius O (eds) *Weather extremes during the past 140 years*, *Geographica Bernensia*, vol G89, pp 35–43. <https://doi.org/10.4480/GB2013.G89.04>
- Tomczak G (1955) Was lehrt uns die Holland-Sturmflut 1953. *Die Küste Doppelheft* 1/2 3. Boyens, Heide, Holstein, pp 78–95
- Wadey MP, Haigh ID, Nicholls RJ, Brown JM, Horsburgh K, Carroll B, Gallop SL, Mason T, Bradshaw E (2015) A comparison of the 31 January–1 February 1953 and 5–6 December 2013 coastal flood events around the UK. *Front Mar Sci* 2. <https://doi.org/10.3389/fmars.2015.00084>
- WAMDI (1988) The WAM model—a third generation ocean wave prediction model. *J Phys Oceanogr* 18:1775–1810. [https://doi.org/10.1175/1520-0485\(1988\)018<1775:twmtgo>2.0.co;2](https://doi.org/10.1175/1520-0485(1988)018<1775:twmtgo>2.0.co;2)
- Westerink JJ, Luettich RA, Feyen JC, Atkinson JH, Dawson C, Roberts HJ, Powell MD, Dunion JP, Kubatko EJ, Pourtaheri H (2008) A basin- to channel-scale unstructured grid hurricane storm surge model applied to southern Louisiana. *Mon Weather Rev* 136:833–864. <https://doi.org/10.1175/2007mwr1946.1>
- Wolf J, Flather RA (2005) Modelling waves and surges during the 1953 storm. *Philos Trans R Soc A Math Phys Eng Sci* 363:1359–1375. <https://doi.org/10.1098/rsta.2005.1572>
- Zijlema M (2010) Computation of wind-wave spectra in coastal waters with SWAN on unstructured grids. *Coast Eng* 57:267–277. <https://doi.org/10.1016/j.coastaleng.2009.10.011>